Jurnal Polimesin
Department of Mechanical Engineering
State Polytechnic of Lhokseumawe
http://e-jurnal.pnl.ac.id/polimesin
e-ISSN : 2549-1999 No. : 6 Month : December
p-ISSN : 1693-5462 Volume : 23 Year : 2025

Processing dates: received on 2025-9-03, reviewed on 2025-11-16, accepted on 2025-12-06 and online availability on 2025-12-31

The effect of flap thickness on the hydrodynamic performance of an oscillating wave surge converter

James Julian[1,*], Rasya Aulia Nathania Nisa[1], Fitri Wahyuni[1], Riki Hendra Purba[1], Fathin Muhammad Madhudhu[2], Elvi Armadani[3]

[1]Department of Mechanical Engineering, Universitas Pembangunan Nasional Veteran Jakarta, Jakarta 12450, Indonesia
[2]Department of Naval Architecture, Universitas Pembangunan Nasional Veteran Jakarta, Jakarta 12450, Indonesia
[3]Department of Industrial Engineering, Universitas Pembangunan Nasional Veteran Jakarta, Jakarta 12450, Indonesia
*Corresponding author: zames@upnvj.ac.id

Abstract

With the growing demand for energy and the need to transition to renewable sources, ocean wave energy presents great potential. The Oscillating Wave Surge Converter (OWSC) is a promising technology due to its near-shore applicability, structural simplicity, and robust design. This study systematically investigates the effect of flap thickness on the dynamic performance of a hinge-mounted OWSC using the Boundary Element Method (BEM). The research models the hydrodynamic interactions and analyzes the effects of three different flap thicknesses on key metrics, including maximum angle deviation, angular velocity, torque, and power capture. The results indicate that all flap variations demonstrate stable oscillatory movement, but greater flap thickness reduces the maximum angle deviation due to increased inertia and hydrostatic pressure. A resonant peak was observed for all thicknesses at a wave period of 1.3 seconds, where energy transfer was maximized. At this frequency, the thickest flap achieved the highest efficiency (78.94%), followed by the intermediate (77.50%) and thinnest (70.77%) variations. The findings suggest that while flap thickness influences efficiency, the primary factor for maximizing energy capture is the alignment of the wave period with the device's natural frequency.

Keywords:
BEM, hydrodynamic, interaction, OWSC, wave energy.

Nomenclature

ϕ_I	: fluid velocity potential
ϕ_D	: fluid diffraction potential
ϕ_R	: fluid radiation potential
M_s	: mass matrix
M_a	: added mass matrix
C	: damping matrix
K	: stiffness matrix
X	: response motion
F	: wave exciting force
η	: free surface elevation
k	: number of waves
h	: wave height
ωt, $\omega(t)$	: angular velocity function over time
$\tau(t)$	: torque function over time
C_g	: group velocity
C_p	: phase speed
$Width$	: flap width
r	: grid refinement ratio
$\bar{p}$	: convergence order
f_1	: simulation result with fine mesh
f_2	: simulation result with medium mesh
f_3	: simulation result with coarse mesh
GCI	: grid convergence index
F_s	: factor of safety
$\in$	: absolute error
$fr_{h=0}$	: true error

1 Introduction

Over the last several decades, technological advancements have led to increased development and economic growth in many countries. However, this growth in industrialization has led to a surge in energy demand, increasing carbon emissions. For instance, Li *et al.* observed that some coastal East and Southeast Asian nations undergoing significant economic development also exhibit high energy consumption and substantial CO_2 emissions. With the growing concern about climate change, actions on transitioning to renewable energy as a way to cut down carbon emissions have to be done immediately. One type of renewable energy that has great potential is ocean wave energy. In East and Southeast Asia alone, the net wave power source total is estimated to be up to 440 GW [1].

A Wave Energy Converter (WEC) is a device that harnesses the kinetic and potential energy of sea waves to generate electricity. Historically, WEC development has been a century-long endeavor, evolving from early patents in the 19th century to the first small-scale buoys in the mid-20th century [2]. Modern WEC technology has since diversified into several primary classifications based on its operating principles and location. These include Oscillating Water Columns (OWCs), which use a closed air chamber to drive a turbine; point absorbers, which are small floating buoys that heave and pitch in all wave directions; and attenuators, which are long, snake-like structures that lie parallel to waves to capture energy from their flexing joints [3], [4], [5]. Among these diverse technologies, the Oscillating Wave Surge Converter (OWSC) stands out for its near-shore applicability, structural simplicity, and ability to effectively harness the surging wave motion [6].

OWSCs are particularly favored for their robust mechanical design, ease of maintenance, and high-power density in coastal environments [7]. The OWSC typically consists of a hinged flap mounted near the seabed or a breakwater that pivots under the force of surging waves. This rotational motion is then converted into usable electricity via a Power Take-Off (PTO) system [4]. Significant research has been conducted on the hydrodynamics of OWSCs to improve their performance and efficiency. For example, several studies have focused on optimizing the PTO system to enhance power output, with Liu *et al.* demonstrating that adjusting the PTO system towards a near-resonance condition significantly boosts the Capture Width Ratio (CWR) under regular waves, and multi-objective optimization under irregular waves favors a thin and tall OWSC profile (high axis depth and low thickness) as the optimal design for balancing CWR maximization and structural mass minimization [6], [8]. Furthermore, Vargas *et al.* analyzed the influence of the bottom slope on the dynamics of a two-dimensional OWSC, concluding that mild slopes are the ideal region for installation [9]. Similarly, Lin & Pei focused on how plate geometry design impacts wave energy conversion, confirming

the importance of height and width ratios for device efficiency [10]. Another study by Cui *et al.* examined the influence of various cross-sectional shapes of the flap on device performance, identifying the rectangular configuration as the most effective for energy capture [11]. These collective efforts have established that both structural geometry and operational parameters are crucial to OWSC performance. Nonetheless, these studies lack in discussing the influence of individual dimensions of the flap, which is a fundamental part of the device.

To ensure proper converter performance and promote material efficiency, it is critical to identify the optimum parametric structure of each part of the device. As a result, it is not only inexpensive to manufacture but also performs well. Flap structure is a fundamental part of OWSC devices, and studies regarding some aspects of it have been conducted extensively. However, a comprehensive parametric investigation into flap thickness has been largely absent from the literature. To address this knowledge gap, the present study systematically examines the effect of flap thickness on key dynamic performance metrics in a hinge-mounted OWSC. This study aims to assist in configuring the ideal flap thickness for OWSC devices to produce the optimal results.

2 Research methodology

2.1 Geometry

OWSC is a type of WEC that captures the horizontal components of waves to drive a piston, which then powers a turbine that generates electricity. This type of WEC consists of a flap that harvests the horizontal wave energy and a hinge that translates the wave energy into an oscillatory movement needed to power the turbine [9], as shown in Fig. 1. This study investigates the hydrodynamic effect as a result of varying flap thickness configurations while keeping the height, width, and density constant at values presented in Table 1. The thickness configurations can be seen in Fig. 2(b), in which the dimensions of each thickness are shown in Table 1. The geometry used in this study follows the model used in an experimental study conducted by Wei et al. (2016). This is done not only as a validation reference to maintain data actualization, but also because the model used is compatible enough to be calculated with the Boundary Element Method (BEM) numeric method.

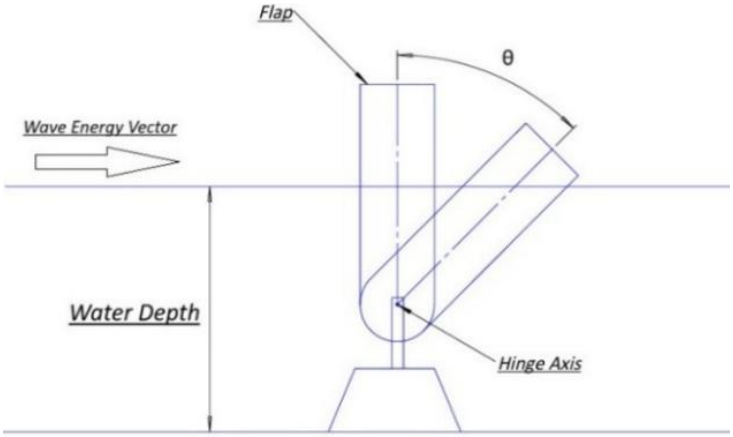

Fig. 1. Mechanism of an oscillating wave surge converter.

Table 1. Geometric properties of the flap variations

Variations	Height (m)	Width (m)	Thickness (m)	Mass (kg)	Water depth (m)
Thickness 1			0.088	4.270	
Thickness 2	0.31	0.646	0.100	4.861	0.305
Thickness 3			0.120	5.810	

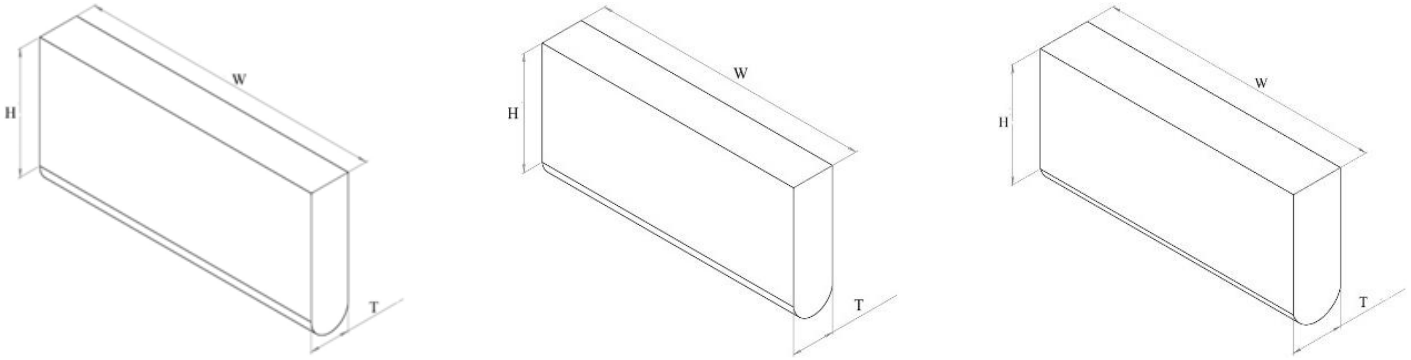

(a) (b) (c)

Fig. 2. Visualization of thickness variations, (a) thickness 1 geometry, (b) thickness 2 geometry, (c) thickness 3 geometry.

2.2 Governing equation

A set of numerical techniques commonly used to model the interactions between sea waves and OWSC devices was employed to support this research. This set of numerical techniques is known as the BEM, which consists of the potential flow equation involving the Laplace and Bernoulli equations to calculate the forces and torques exerted on the flap. This method assumes the fluid flow to be incompressible, in-viscid, and irrotational [12]. The BEM primarily emphasizes the dynamics, motion, and characteristics of structures in relation to their interaction with the surrounding fluid, which is best, suited for this study [13]. Consequently, the assumption that the fluid is irrotational, in-viscid, and incompressible is not only justifiable but also contributes to a reduction in computational complexity [14].

In this numerical technique, the wave force is formulated by Eq. (1) in accordance with the potential flow theory. Then, the motion of the flap is formulated by Eq. (2) and Eq. (3), which are divided into a frequency-domain and a time-domain scheme. In the scheme of the frequency domain, Eq. (2) calculates the hydrodynamic characteristics exerted on the flap as a single body in various wave conditions, which includes nonlinear hydrostatic, Froude-Krylov forces, added mass, and damping matrix. Meanwhile, in the time domain, the response of the flap towards the wave force is observed as a mechanical system unit in a certain time range, as represented in Eq. (3). Fig. 3 shows the scheme of this numerical technique, in which the potential flow theory provides wave force data needed to calculate the motion of the structure. Afterward the motion is first calculated in the frequency domain, which will provide the mass and damping matrix needed to calculate the motion in the time domain.

$$\nabla^2\phi(x,y,z,t) = \phi_I(x,y,z,t) + \phi_D(x,y,z,t) + \phi_R(x,y,z,t) = a_w\varphi(x,y,z,t)e^{-i\omega t} \quad (1)$$

$$\begin{bmatrix} -\omega^2(M_s + M_a(\omega)) \\ -i\omega C(\omega) + K \end{bmatrix} X(\omega) = F(\omega) \quad (2)$$

$$M\ddot{X}(t) + C\ddot{X}(t) + KX(t) + C_h\dot{X}(t) = F(t) \quad (3)$$

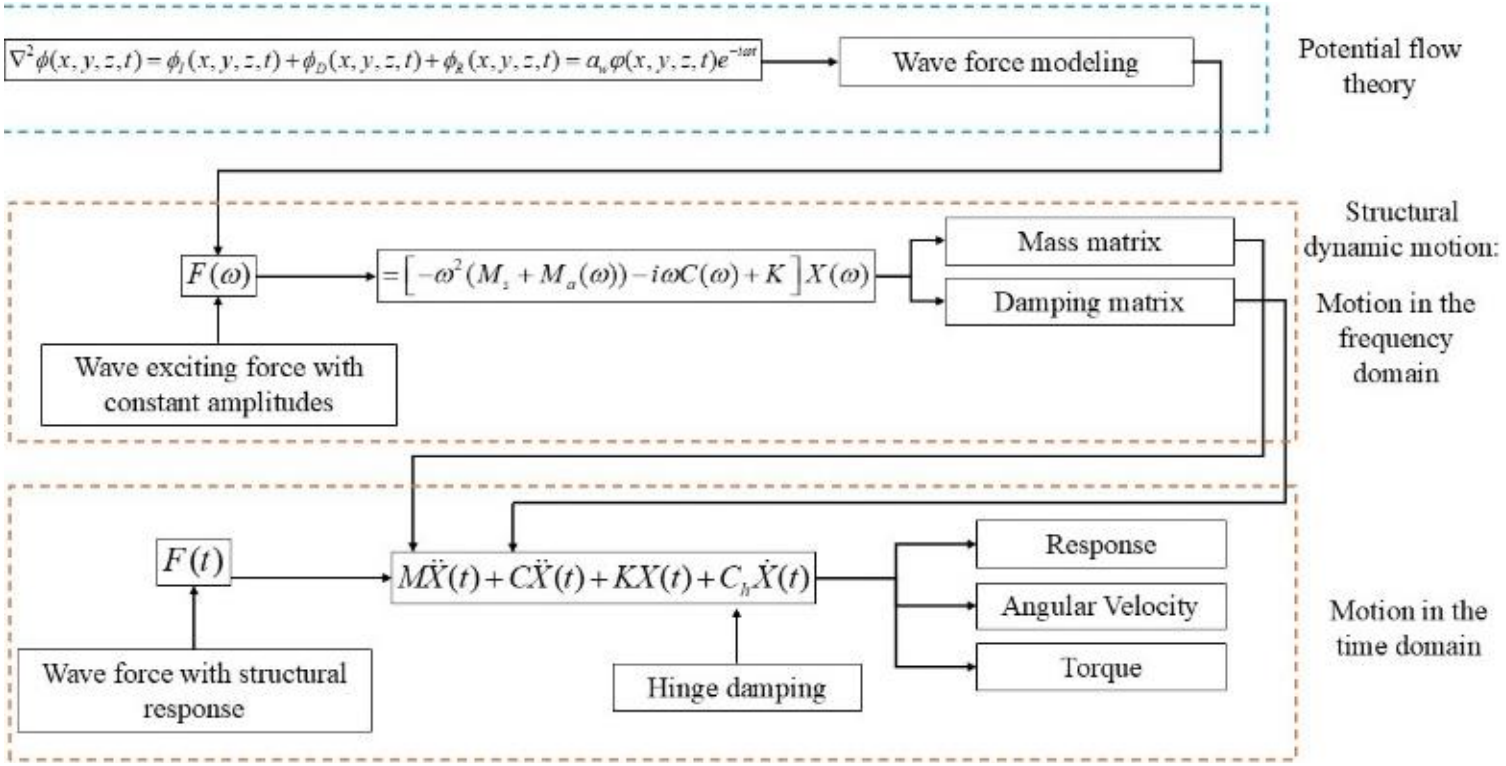

Fig. 3. Numerical scheme of boundary element method.

2.3 Meshing and boundary conditions

Meshing is achieved on the geometry in order to support the numerical methods. Meshing is the process of discretizing a continuous domain into individual elements, which allows for the assignment of governing equations. The quality of the mesh is crucial, as it directly impacts the accuracy of the simulation results, as well as their convergence and stability. In this study, the type of mesh used is a quadrilateral mesh in which the flap geometry is interpreted as a surface domain and then divided into smaller quadrilateral elements. The configuration of the mesh is represented in Fig. 4.

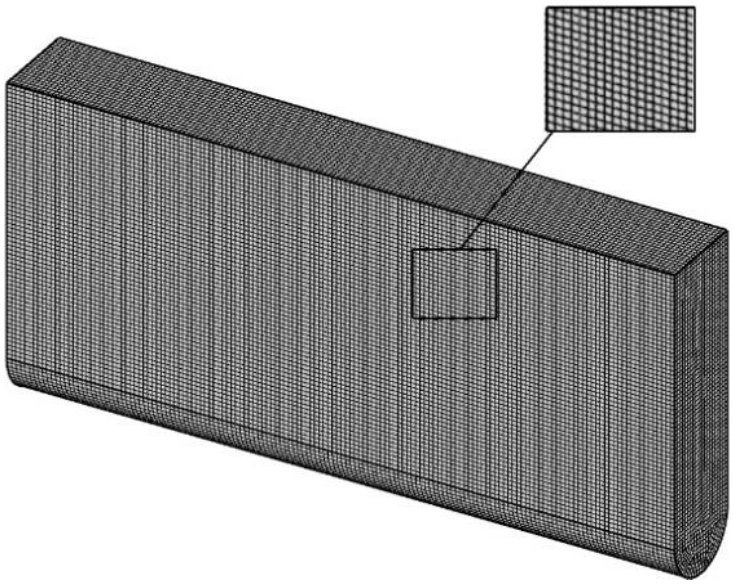

Fig. 4. Mesh configuration of the study.

Furthermore, boundary conditions are established to represent the real-world interaction between ocean waves and the flap structure. The sea wave modeled in this study is categorized as a regular wave with constant amplitude. Variation in wave period, specified in Table 2, is applied to thoroughly examine the hydrodynamic characteristics and performance of the device. The modeling of the sea wave is done by using the Airy Wave Theory as depicted in Eq. (4) [12].

$$\eta(x,t)=\frac{h}{2}\cos(\omega t-k(x\cos\theta)) \tag{4}$$

Table 2. Configurations of the sea wave

Wave configuration		
Amplitude (m)	Period (s)	Wavelength (m)
0.1	1.1	1.581
	1.3	1.975
	1.5	2.357
	1.7	2.730
	1.9	3.098
	2.1	3.462
	2.3	3.823
	2.5	4.181
	2.7	4.538
	2.9	4.893

In examining the hydrodynamic characteristics, the interaction between the OWSC device and the sea wave is analyzed. On the other hand, the hydrodynamic performance of the device is achieved through analyzing several power data, such as the power of the wave energy source and the mechanical power of the device, which are calculated in Eq. (5) and Eq. (6), respectively. In calculating the wave energy source power, the group velocity of the wave is described in Eq. (7). Furthermore, the device's ability to capture power is also calculated with the capture width ratio equation, as depicted in Eq. (8), which also describes the device's efficiency [15].

$$P_w=\frac{1}{2}\rho g A^2 C_g \tag{5}$$

$$P_{OWSC}=|\tau(t)\times\omega(t)| \tag{6}$$

$$C_g=\frac{1}{2}C_p\left\{1+\frac{kD}{\sinh kD\times\cosh kD}\right\} \tag{7}$$

$$CWR = \frac{P_{OWSC}}{P_W \times Width} \quad (8)$$

2.4 Mesh independence test

The mesh independence test is a method used to determine the error values of meshes and verify that each one lies within the defined convergence range. The independence test method used in this study follows the method that is introduced by Roache [16]. In this method, three mesh configurations with variations in mesh element number are made. The variations in element number include 13352, 20642, and 30462. These mesh variations are classified into three categories, which are coarse, medium and fine. The number of mesh elements is constrained by the grid refinement ratio set in Eq. (9). In this testing method, a sample of data from each mesh variation is taken. The sample data is the maximum absolute amplitude in the wave parameter of 0.1 meters and a period of 1.9 seconds. The order value is evaluated with Eq. (10). Moreover, Eq. (11) and (12) support the error calculation in each mesh variation. These equations are known as the Grid Convergence Index (GCI) and are divided into two categories, namely GCI_{fine} and GCI_{coarse}. GCI_{fine} evaluates the error value amongst fine and medium mesh, while GCI_{coarse} evaluates that amongst medium and coarse mesh. In order to ensure the accuracy of the error value, the calculation must be done within the convergence area (Eq. (13)). This is done by testing the GCI results with Eq. (14). Eq. (15) evaluates the result of the test, which then can be used to obtain the error value of each mesh variation. Table 3 shows the result of the mesh independence test. According to the result, the fine mesh variation exhibits the least error, thus making it the ideal configuration for conducting the study.

Table 3. Mesh independence test results

Mesh category	Fine	Medium	Coarse
Maximum response (m)	57.64648438	57.64332581	57.63967514
$\bar{p}$		0.357096663	
r		1.5	
GCI_{fine}		0.044%	
GCI_{coarse}		0.0508%	
$\frac{GCI_{fine}}{GCI_{coarse}}$		1.000	
$f_{rh}=0$		57.66676	
Error	0.03516%	0.04063%	0.04696%

$$r = \frac{h_2}{h_1} \quad (9)$$

$$\bar{p} = \frac{\ln\left(\frac{f_3 - f_2}{f_2 - f_1}\right)}{\ln(r)} \quad (10)$$

$$GCI_{fine} = \frac{F_s \,|\in|}{(r^{\bar{p}} - 1)} \quad (11)$$

$$GCI_{coarse} = \frac{F_s \,|\in| \, r^{\bar{p}}}{(r^{\bar{p}} - 1)} \quad (12)$$

$$\in = \frac{f_{n+1} - f_n}{f_n} \quad (13)$$

$$\frac{GCI_{fine}}{GCI_{coarse}} \approx 1 \quad (14)$$

$$fr_{h=0} = f_1 + \frac{(f_1 - f_2)}{(r^{\bar{p}} - 1)} \quad (15)$$

3 Results and discussion

3.1 Validation

Data validation analysis was conducted prior to discussing the main data of the study. This is done to ensure the numerical results match actual conditions. This analysis is executed by comparing the flap motion response data obtained through numerical methods with experimental data conducted by Wei *et al.* [17]. This data is taken at a wave parameter of A = 0.1 m and T = 1.9 s. Fig. 5 shows the comparison between numerical and experimental data. As can be seen from the figure, the numerical data closely follow the experimental data, specifically in the aspect of frequency and phase angle. Although there are slight discrepancies in amplitude, the overall trend and result are similar enough to ensure the validity of the numerical method.

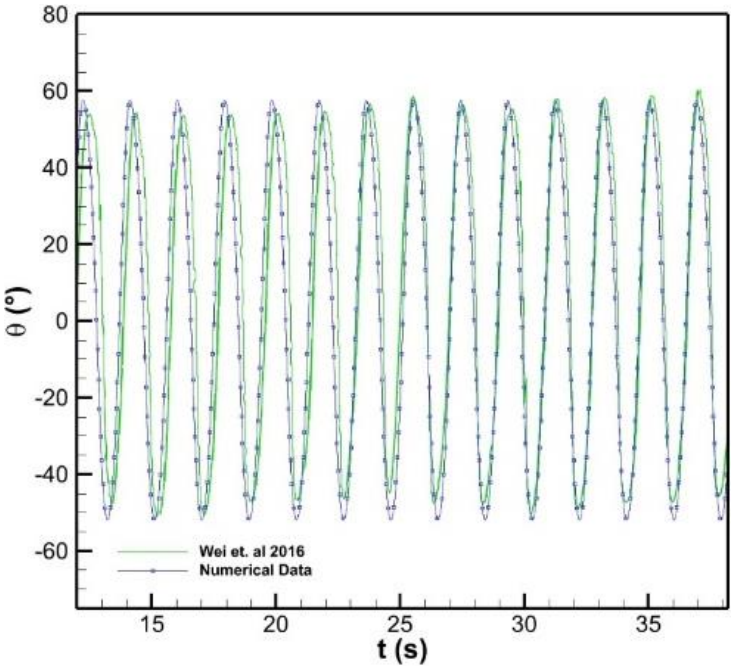

Fig. 5. Comparison of numerical data with experimental data.

3.2 Data analysis

3.2.1 Hydrodynamic parameters in the time domain

Fig. 6(a) describes the motion response data from each thickness variation when subjected to incoming sea waves with an amplitude of 0.1 m and a period of 1.9 seconds. In the OWSC device, the flap is constrained at one degree of freedom by the hinge. Therefore, when the incoming sea wave drives the hinge-mounted flap, the flap experiences an angular deviation from its equilibrium position. The continuous nature of the sea waves causes the displacement of the flap to be oscillatory. It can also be seen in the figure that there exists a slight difference in amplitudes and phase time in all three variations. Thickness variation affects its amplitude such that Thickness 1 exhibits the highest amplitude, followed by Thickness 2, then Thickness 3 with the lowest amplitude. These observations indicate that flap thickness influences the maximum angle deviation, with greater thickness resulting in a reduced deviation magnitude as well as a delayed phase time. When the thickness of the flap is increased, so do the geometric properties of the flap, such as volume and surface area. This increase in volume and surface area proportionally influences the factors that inhibit the deviation of the flap, which are inertia

and hydrostatic pressure. Inertia impedes the flap's motion because the added volume increases its mass and thus its rotational inertia, requiring more torque to achieve equivalent angular displacement (i.e., increasing the moment of inertia reduces angular acceleration for a given torque). On the other hand, hydrostatic pressure exerts a stronger restoring moment, as a larger submerged surface area yields a greater buoyancy-induced torque that resists angular displacement [18]. Added volume of the structure translates to an increase in mass, and this consequently increases the inertia. In the context of hydrostatic pressure, a larger surface area results in a larger submerged area that are subjected to hydrostatic pressure. It can be concluded that added thickness leads to a gain in inertia and hydrostatic pressure, which are inhibiting factors that reduce the angular deviation of the flap.

To further illustrate the interaction between the sea waves and the flap, the angular velocity and torque are represented in Fig. 6(b) and Fig. 6(c). The torque and angular velocity exhibit a phase difference, implying that the directions of their respective vectors are opposed. This is expected since the torque functions as a restoring force that seeks to return the flap to its equilibrium position. Thus its vector will oppose that of the increasing angular velocity caused by the incoming wave. These parameters also exhibit an oscillatory behavior that appears nearly sinusoidal, indicating a regular periodic excitation consistent with the uniform wave excitation. The phase time and amplitude of the thickness fluctuations also differ from one another. The fastest phase time is displayed by Thickness 1, which is followed by Thickness 2 and Thickness 3. The lowest amplitude, however, is shown by Thickness 1, which is followed by Thickness 3 and Thickness 2, which has the maximum amplitude in angular velocity and torque in this specific wave parameter. These behaviors in angular velocity and torque will then affect the power of the device.

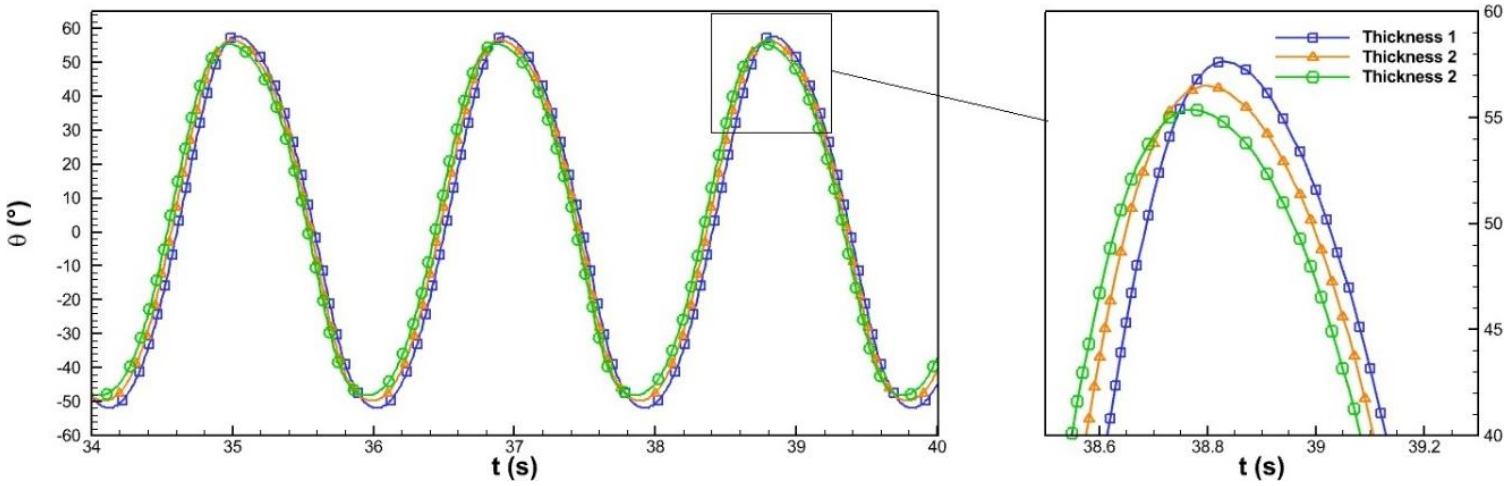

(a)

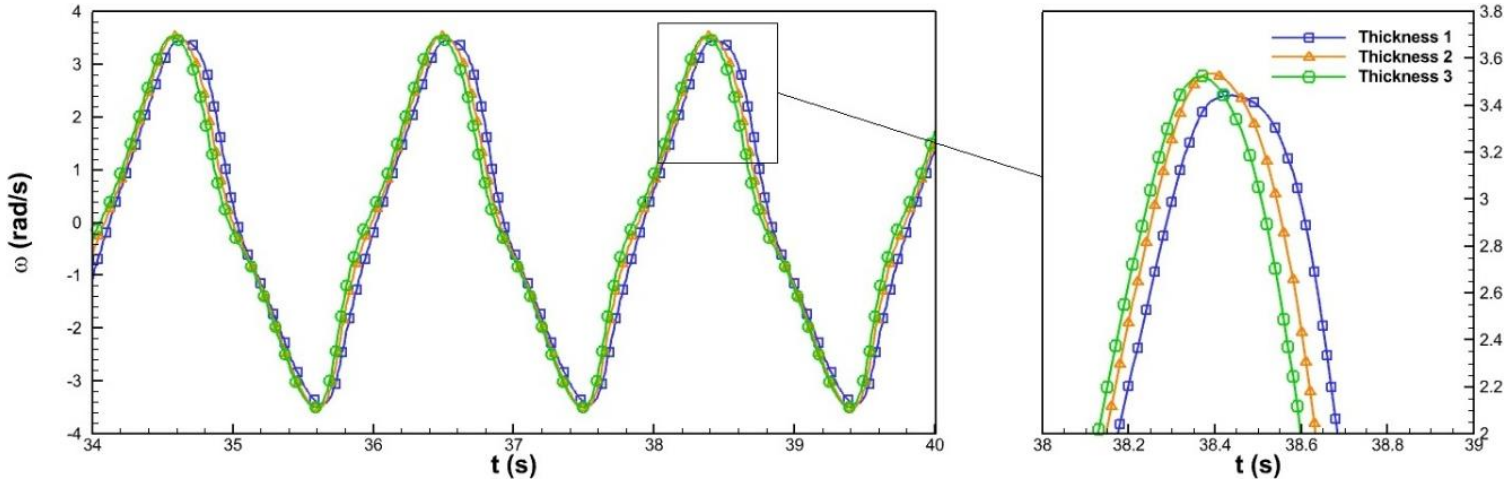

(b)

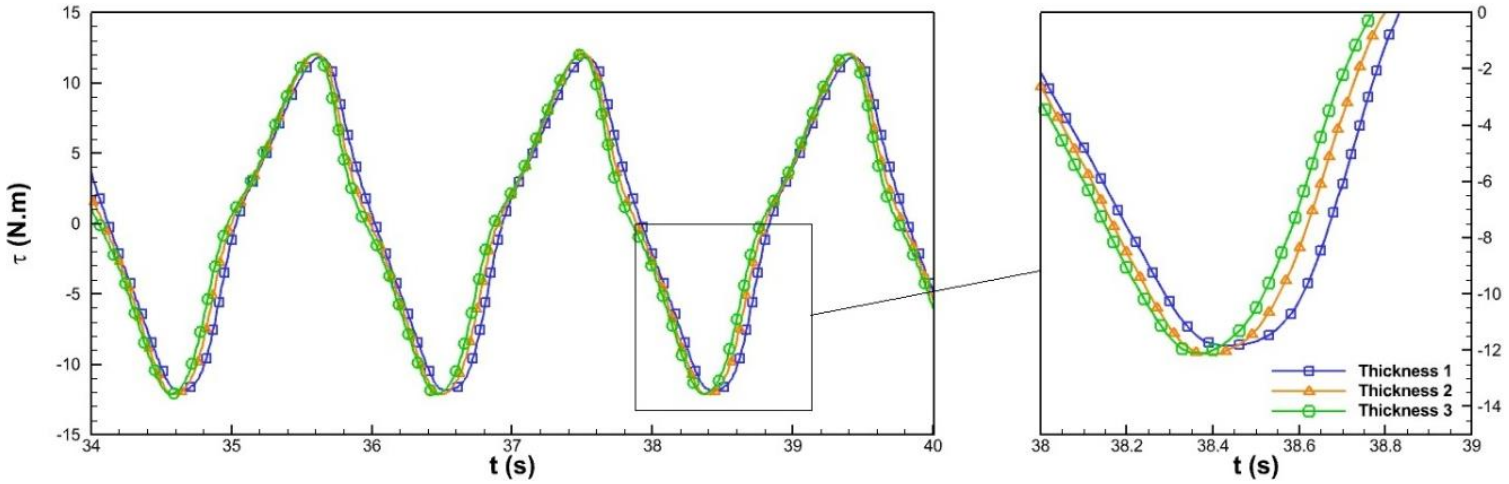

(c)

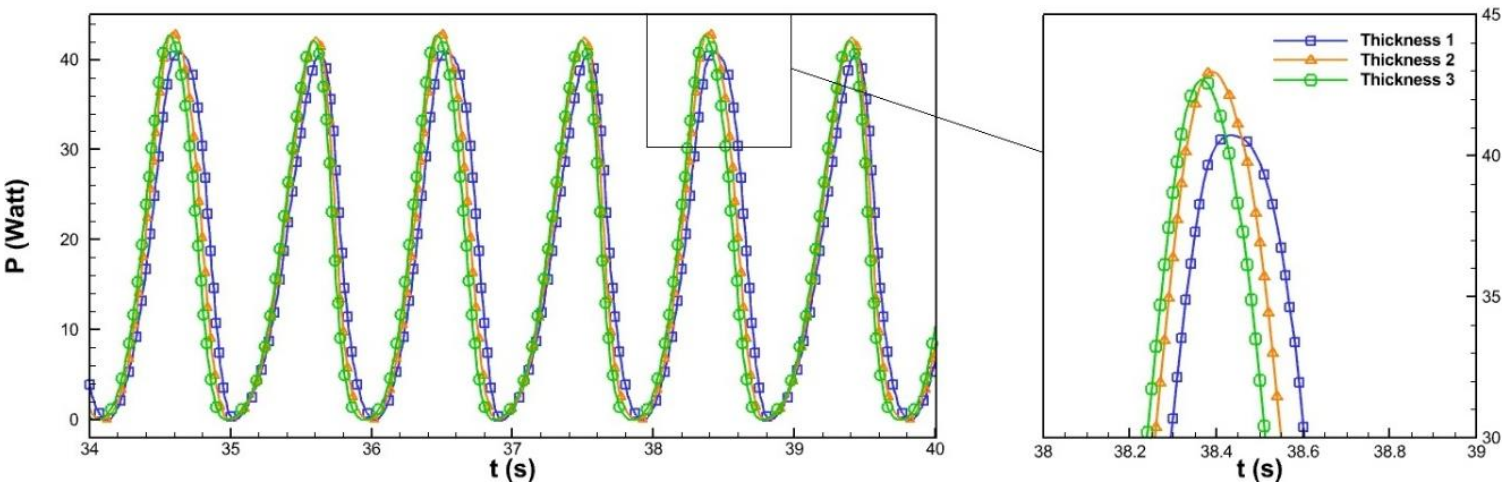

(d)

Fig. 6. Hydrodynamic parameter results of all variations at parameter a = 1 m and t = 1.9 s, (a) motion response, (b) angular velocity, (c) torque, and (d) power.

Regarding the power produced by the device, shown in Fig. 6(d), it is influenced by torque and angular velocity as it is the absolute product of both parameters. The phase difference between the torque and angular velocity causes fluctuations in instantaneous power, but because the absolute product is considered, the power remains largely positive. This results in an oscillatory power curve that reflects the harmonic nature of the wave excitation acting on the system. The periodic variations arise from the cyclic wave forcing and the phase difference between torque and velocity. The power between the variations shows the same pattern as angular velocity and torque, with Thickness 1 having the smallest amplitude, next being Thickness 3 and Thickness 2 with the highest amplitude. Then, in terms of phase time, Thickness 1 has the longest phase duration, followed by Thickness 2 and Thickness 3, which have the slowest phase times. Overall, the data indicate that despite phase mismatches, the structure consistently extracts net positive power from the waves, with the oscillation mean representing the effective energy capture efficiency.

3.2.2 Hydrodynamic parameters in the period domain

The effect of flap thickness shows more evidently in terms of maximum response, average angular velocity, and average torque at different sea wave periods as depicted in Fig. 7. From the perspective of maximum response, Thickness 1 has the largest trend, followed by Thickness 2, and Thickness 3 with the lowest trend; it is worth noting that there exists a peak in maximum response magnitude for all thickness variations when subjected to a wave period of 1.3 seconds.

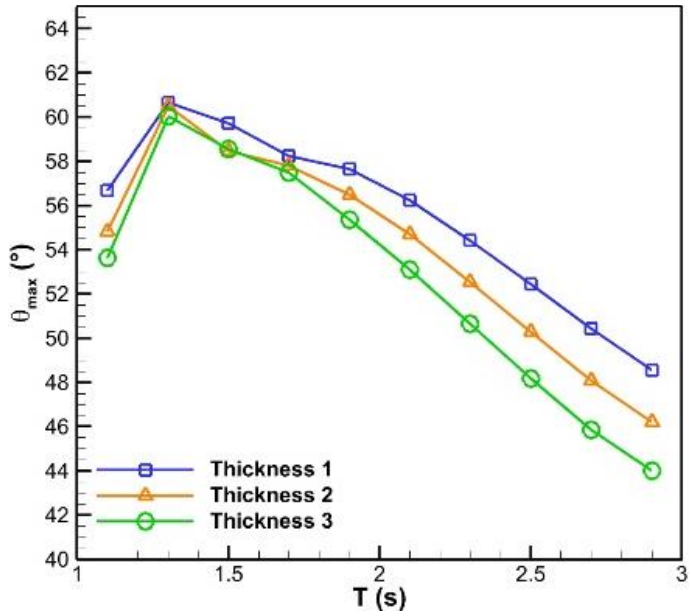

(a)

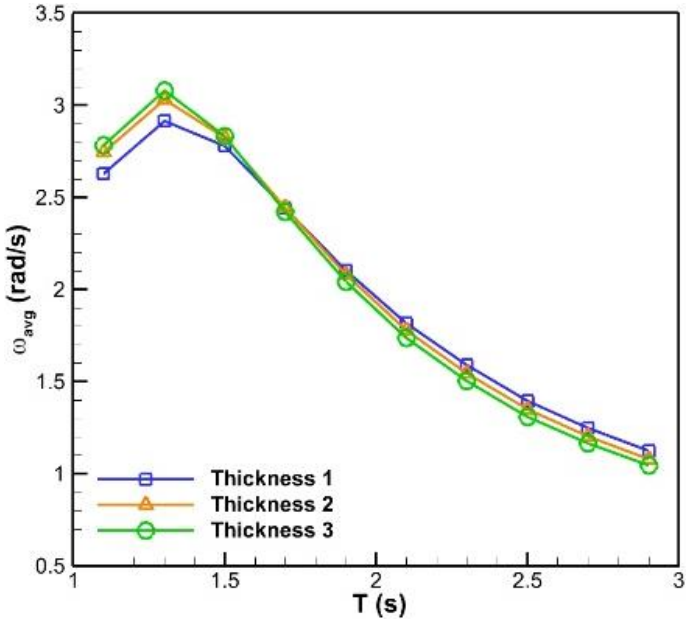

(b)

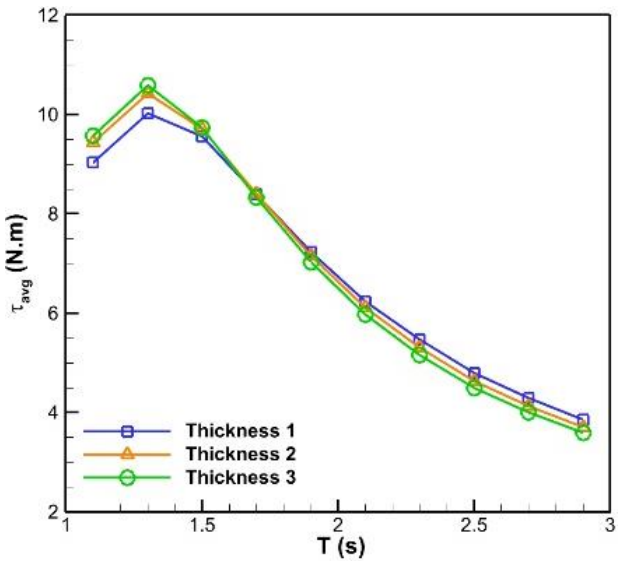

(c)

Fig 7. Comparison of hydrodynamic parameters between all variations at different wave periods, (a) maximum amplitude, (b) average angular velocity, (c) average torque.

This behavior is similar to that of the response data in the time domain as discussed previously. This implies that the influence of added mass affects the maximum response in all wave periods as well.

In the context of averaged angular velocity and averaged torque, as presented in Fig. 7(b) and Fig. 7(c), all thickness variations experience a peak at a period of 1.3 seconds. This rising trend suggests an influence from the phenomenon of resonance, where the energy absorbed by the structure is significantly maximized when the structure's motion is in phase with the wave excitation force [8], [19]. Therefore, based on this trend in the hydrodynamic characteristics (response, angular velocity, and torque), it can be concluded that the natural period of the flap structure likely tends toward this wave period of 1.3 seconds. This resonance effect enables efficient energy transfer from the waves to the structure, resulting in the simultaneous achievement of the highest angular velocity and torque responses. Notably, the thickest flap (Thickness 3) exhibits the greatest peak response in this region, since its increased stiffness and hydrodynamic loading allow it to extract more energy from the resonant waves.

On the other hand, there exists a decline in the same parameters as wave periods deviate away from 1.3 seconds ($T < 1.3$ s and $T > 1.3$ s). At shorter wave periods ($T < 1.3$ s), the incident waves oscillate at a frequency higher than the natural frequency of the flap. In this period range, the flap cannot fully keep pace with the rapid oscillations of the waves, resulting in inefficient transfer of energy, leading to moderate torque and consequently reduced angular velocity. Meanwhile, at longer wave periods ($T > 1.3$ s), the wave oscillations occur more slowly than the flap's natural response. As a result, the flap is unable to sustain sufficient momentum transfer from the waves, leading to a reduction in angular velocity despite the longer oscillation period. Similarly, torque decreases because the slower oscillations produce weaker dynamic forcing on the flap. In the Thickness 3 variation, this reduction is more pronounced, such that while its higher stiffness enhances resonance at shorter periods, it also causes the flap to be less responsive to the slower oscillations associated with longer periods. As a result, Thickness 3 variations transition from producing the highest magnitude in angular velocity and torque near resonance to the lowest at longer periods, highlighting the trade-off between stiffness-enhanced resonance and flexibility-driven responsiveness.

Fig. 8 reveals the comparison of the averaged power between the three thickness variations. The power output of the flap system is directly determined by the absolute product of torque and angular velocity. In other words, when either of these parameters is maximized, the resulting power is also elevated; inversely, reductions in both lead to diminished power generation. This relationship explains the observed power trend in the graph, where all thickness variations reach a maximum at a wave period of 1.3 seconds, coinciding with the resonance effect in which both angular velocity and torque are amplified. Beyond this point, as the wave period increases, both torque and velocity decrease due to the mismatch between wave excitation and the flap's natural period, resulting in progressively lower power. The trend between the three thickness variations also follows that of both averaged angular velocity and averaged torque, wherein Thickness 3 produces the highest averaged power at a wave period around the resonance area and starts to decrease until it eventually becomes the variation with the least averaged power as the wave period becomes longer. This further highlights the strong relationship between angular velocity, torque and power.

Concerning the efficiency of the device in converting the incident wave power into usable output power, it is represented by the CWR as depicted in Table 4. It is also defined as the ratio between the device's power output and the available wave power normalized by the flap width [20]; since the width is kept constant, the CWR is directly proportional to the output power. The table shows that CWR reaches its maximum at a wave period of 1.3 seconds for all thickness variations, where the resonance condition enhances torque and angular velocity, thereby maximizing power extraction. Beyond this point, as the wave period increases, the CWR decreases steadily due to the reduced interaction between the wave excitation and the flap's natural frequency, leading to lower efficiency in energy capture. Moreover, the comparison of CWR values between the thickness variations follows that of the averaged power, wherein at shorter wave periods, Thickness 3 possesses the highest efficiency around the resonance, but at longer periods, it is the lowest. The table confirms this trend numerically. For instance, at 1.3 seconds, Thickness 3 achieves the highest efficiency of 78.94%, followed by Thickness 2 with 76.50%, and Thickness 1 with 70.77%, demonstrating that the resonance effect enables efficient energy transfer with thicker flaps extracting slightly more energy. However, at longer periods such as 2.9 seconds, all thicknesses converge to low efficiency, with Thickness 3 possessing the lowest efficiency of 7.40%. This further supports the conclusion that resonance strongly governs the energy capture performance of the system. Overall, the structures demonstrate their best performance around the resonance period, with thicker variations yielding slightly higher CWR values, indicating that thickness influences efficiency, but the dominant factor remains the alignment of the wave period with the flap's natural response, highlighting the critical role of resonance in maximizing wave energy conversion.

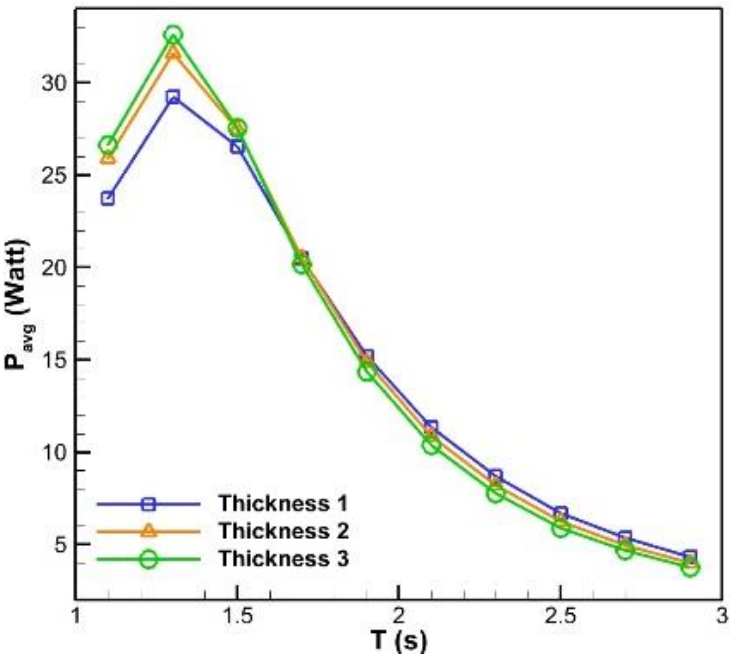

Fig. 8. Comparison of the average power output between the thickness variations.

Table 4. Comparison of capture width ratio between the thickness variations

Period (s)	Capture width ratio		
	Thickness 1	Thickness 2	Thickness 3
1.1	57.45%	62.73%	64.46%
1.3	70.77%	76.50%	78.94%
1.5	64.29%	66.45%	66.70%
1.7	46.55%	46.72%	45.90%
1.9	33.04%	32.34%	31.25%
2.1	23.90%	22.94%	21.90%
2.3	17.90%	16.90%	15.97%
2.5	13.52%	12.65%	11.91%
2.7	10.69%	9.92%	9.31%
2.9	8.54%	7.88%	7.40%

4 Conclusions

This study investigated the influence of flap thickness on the hydrodynamic performance of an OWSC through a BEM analysis. The results confirm that flap thickness affects the dynamic response of the device, with increased thickness leading to reduced maximum angular deviation due to higher inertia and hydrostatic

pressure due to a gain in inertia and hydrostatic pressure. Through consistent observation, a key finding is that the hydrodynamic characteristics (angular velocity and torque) for all flap variations reaching their peak values at a wave period of 1.3 s. This trend suggests that the natural period of the flap structure tends toward this specific wave period, confirming the critical role of resonance as the most significant factor in maximizing energy capture. At this inferred resonant condition, the thickest flap (thickness 3) achieved the highest efficiency of 78.94%. However, a critical trade-off was also identified: as the wave period deviated from the inferred resonant frequency, the performance of the thicker flap decreased more sharply, highlighting a reduction in its responsiveness to non-optimal wave conditions. In conclusion, while a thicker flap can slightly enhance performance at resonance, the dominant determinant for optimal energy conversion is the precise tuning of the device to the prevailing wave climate.

References

[1] M. Li *et al.*, "State-of-the-art review of the flexibility and feasibility of emerging offshore and coastal ocean energy technologies in East and Southeast Asia," *Renewable and Sustainable Energy Reviews*, vol. 162, p. 112404, Jul. 2022, doi: 10.1016/J.RSER.2022.112404.

[2] A. F. O. de Falcão, "Wave energy utilization: A review of the technologies," *Renewable and Sustainable Energy Reviews*, vol. 14, no. 3, p. 899, Jan. 2010, Accessed: Aug. 18, 2025. [Online]. Available: https://commons.wmu.se/lib_articles/62

[3] H. Bouhrim, A. El Marjani, R. Nechad, and I. Hajjout, "Ocean Wave Energy Conversion: A Review," *J Mar Sci Eng*, vol. 12, no. 11, Nov. 2024, doi: 10.3390/JMSE12111922.

[4] D. Golbaz *et al.*, "Layout and design optimization of ocean wave energy converters: A scoping review of state-of-the-art canonical, hybrid, cooperative, and combinatorial optimization methods," *Energy Reports*, vol. 8, pp. 15446–15479, Nov. 2022, doi: 10.1016/J.EGYR.2022.10.403.

[5] Z. M. Yusop, M. Z. Ibrahim, M. A. Jusoh, A. Albani, and S. J. A. Rahman, "Wave-Activated Body Energy Converter Technologies: A Review," *Journal of Advanced Research in Fluid Mechanics and Thermal Sciences*, vol. 76, no. 1, pp. 76–104, 2020, doi: 10.37934/ARFMTS.76.1.76104.

[6] Y. Liu, N. Mizutani, Y. H. Cho, and T. Nakamura, "Nonlinear hydrodynamic analysis and optimization of oscillating wave surge converters under irregular waves," *Ocean Engineering*, vol. 250, p. 110888, Apr. 2022, doi: 10.1016/J.OCEANENG.2022.110888.

[7] E. Amini *et al.*, "Comparative Study of Oscillating Surge Wave Energy Converter Performance: A Case Study for Southern Coasts of the Caspian Sea," *Sustainability 2021, Vol. 13, Page 10932*, vol. 13, no. 19, p. 10932, Oct. 2021, doi: 10.3390/SU131910932.

[8] Y. Liu, Y. H. Cho, N. Mizutani, and T. Nakamura, "Study on the resonant behaviors of a bottom-hinged oscillating wave surge converter," *J Mar Sci Eng*, vol. 10, no. 1, Jan. 2022, doi: 10.3390/JMSE10010002.

[9] G. F. Vargas, E. B. C. Schettini, and B. A. Scapin, "Dynamics of an oscillating wave surge converter: an analysis on the influence of the bottom slope," *South Florida Journal of Development*, vol. 4, no. 1, pp. 330–343, Feb. 2023, doi: 10.46932/sfjdv4n1-024.

[10] Y. Lin and F. Pei, "Numerical study on bottom-hinged plate wave energy converter geometry design," *Ocean Engineering*, vol. 260, p. 112050, Sep. 2022, doi: 10.1016/J.OCEANENG.2022.112050.

[11] J. Cui, X. Chen, and S. Dai, "Numerical study on dual oscillating wave surge converter with different cross-section shapes using SPH under regular waves," *Ocean Engineering*, vol. 271, p. 113755, Mar. 2023, doi: 10.1016/J.OCEANENG.2023.113755.

[12] J. N. Newman, "Marine Hydrodynamics, 40th edition," *The MIT Press Cambridge, Massachusetts London, England*, p. 450, 2018, Accessed: Aug. 18, 2025. [Online]. Available: https://mitpress.mit.edu/9780262534826/marine-hydrodynamics/

[13] B. Teng and Y. Gou, "BEM for wave interaction with structures and low storage accelerated methods for large scale computation," *Journal of Hydrodynamics 2017 29:5*, vol. 29, no. 5, pp. 748–762, Oct. 2017, doi: 10.1016/S1001-6058(16)60786-2.

[14] E. J. Sellountos, T. V. Gortsas, and D. Polyzos, "A local domain boundary element method for solving 2D incompressible fluid flow problems," *Eng Anal Bound Elem*, vol. 150, pp. 457–481, May 2023, doi: 10.1016/J.ENGANABOUND.2023.02.012.

[15] B. Drew, A. R. Plummer, and M. N. Sahinkaya, "A review of wave energy converter technology," *Proceedings of the Institution of Mechanical Engineers, Part A: Journal of Power and Energy*, vol. 223, no. 8, pp. 887–902, Dec. 2009, doi: 10.1243/09576509JPE782;PAGE:STRING:ARTICLE/CHAPTER.

[16] P. J. Roache, "Perspective: A Method for Uniform Reporting of Grid Refinement Studies," *J Fluids Eng*, vol. 116, no. 3, pp. 405–413, Sep. 1994, doi: 10.1115/1.2910291.

[17] Y. Wei, T. Abadie, A. Henry, and F. Dias, "Wave interaction with an Oscillating Wave Surge Converter. Part II: Slamming," *Ocean Engineering*, vol. 113, pp. 319–334, Feb. 2016, doi: 10.1016/j.oceaneng.2015.12.041.

[18] M. Kelly, N. Tom, Y.-H. Yu, R. Thresher, and N. Abbas, "Development of the Second-Generation Oscillating Surge Wave Energy Converter With Variable Geometry," Jun. 25, 2017, *OnePetro*. Accessed: Aug. 18, 2025. [Online]. Available: https://dx.doi.org/

[19] H. N. Nguyen, "Is the Velocity Always in Phase with the Wave Excitation Force in Constrained Optimal Control of Wave Energy Converters?," *IFAC-PapersOnLine*, vol. 56, no. 2, pp. 2632–2637, Jul. 2023, doi: 10.1016/J.IFACOL.2023.10.1352.

[20] R. A. Anggara, J. Julian, F. Wahyuni, R. H. Purba, and N. T. Bunga, "Investigation of Flap Dimensional Parameters to Improve Hydrodynamic Performance of Oscillating Wave Surge Converter Device," *Jurnal Asiimetrik: Jurnal Ilmiah Rekayasa & Inovasi*, vol. 7, no. 1, pp. 59–70, Jan. 2025, doi: 10.35814/ASIIMETRIK.V7I1.7911.